Proton energy and scattering angle radiographs to improve proton treatment planning

Biegun, A. K.; Takatsu, J.; Nakaji, T.; van Goethem, M. J.; van der Graaf, E. R.; Koffeman, E.N.; Visser, J; Brandenburg, S

Published in:
Journal of Instrumentation

DOI:
10.1088/1748-0221/11/12/C12015

Proton energy and scattering angle radiographs to improve proton treatment planning: a Monte Carlo study

2016 JINST 11 C12015

(http://iopscience.iop.org/1748-0221/11/12/C12015)

Published by IOP Publishing for Sissa Medialab
Received: *September 30, 2016*
Accepted: *November 21, 2016*
Published: *December 7, 2016*

18th International Workshop on Radiation Imaging Detectors
3–7 July 2016,
Barcelona, Spain

Proton energy and scattering angle radiographs to improve proton treatment planning: a Monte Carlo study

A.K. Biegun,[a,1] **J. Takatsu,**[b] **T. Nakaji,**[b] **M.J. van Goethem,**[a,c] **E.R. van der Graaf,**[a] **E.N. Koffeman,**[d] **J. Visser**[d] **and S. Brandenburg**[a]

[a] *KVI-Center for Advanced Radiation Technology, University of Groningen, Zernikelaan 25, 9747AA Groningen, The Netherlands*
[b] *Department of Radiation Oncology, Graduate School of Medicine, Osaka University 2-2 D10 Yamadaoka, Suita, Osaka, 565-0871, Japan*
[c] *Department of Radiation Oncology, University Medical Center Groningen, University of Groningen Hanzeplein 1, 9700 RB Groningen, The Netherlands*
[d] *National Institute for Subatomic Physics (Nikhef), Science Park 105, 1098 XG Amsterdam, The Netherlands*

E-mail: marek@ipj.gov.pl

Abstract: The novel proton radiography imaging technique has a large potential to be used in direct measurement of the proton energy loss (proton stopping power, PSP) in various tissues in the patient. The uncertainty of PSPs, currently obtained from translation of X-ray Computed Tomography (xCT) images, should be minimized from 3–5% or higher to less than 1%, to make the treatment plan with proton beams more accurate, and thereby better treatment for the patient.

With Geant4 we simulated a proton radiography detection system with two position-sensitive and residual energy detectors. A complex phantom filled with various materials (including tissue surrogates), was placed between the position sensitive detectors. The phantom was irradiated with 150 MeV protons and the energy loss radiograph and scattering angles were studied. Protons passing through different materials in the phantom lose energy, which was used to create a radiography image of the phantom. The multiple Coulomb scattering of a proton traversing different materials causes blurring of the image. To improve image quality and material identification in the phantom, we selected protons with small scattering angles.

A good quality proton radiography image, in which various materials can be recognized accurately, and in combination with xCT can lead to more accurate relative stopping powers predictions.

Keywords: Computerized Tomography (CT) and Computed Radiography (CR); Algoritms and Software for radiotherapy; Image reconstruction in medical imaging; Models and simulations

[1] Corresponding author.

doi:10.1088/1748-0221/11/12/C12015

Contents

1 Introduction

Proton radiography is a novel imaging modality (still under development) that has a large potential to be favourably used in proton radiotherapy treatment. Besides for patient positioning, it can also be used as an additional imaging tool for an accurate determination of proton stopping powers, which are crucial for accurate proton treatment planning.

Proton radiography delivers direct information about the stopping powers of different materials in an imaged object (patient), through which the proton from the beam has passed. Both proton radiography and its 3D extension proton Computed Tomography (pCT) are being developed in various laboratories [1–8]. The spatial resolution of an imaged object measured with proton radiography or pCT is reduced by multiple Coulomb scattering (MCS) and energy loss processes of protons in matter. These processes will affect the position resolution of a proton traversing different materials in the object and will lead to blurred images. The scattering angle of a proton passing through various materials was studied in order to assess the possibilities to reduce this blurring. We investigated the influence of selection of the proton scattering angle on the quality of the reconstructed energy radiograph.

2 Geant4 Monte Carlo simulations

2.1 Proton radiography setup

In this study, we performed Monte Carlo simulations using Geant4 [9], where we implemented the proton radiography setup, as demonstrated in figure 1. A scattered proton beam with proton energy of $E_p = 150\,\text{MeV}$ and a field size of $6 \times 10\ \text{cm}^2$ was used to irradiate a phantom. The phantom (described in more details in section 2.2) was larger and more complex than the one used earlier [6–8]. Considering the increased size of the phantom, the sizes of both ideal position sensitive detectors (100% efficiency, 1 μm thickness filled with air) measuring a trajectory of an

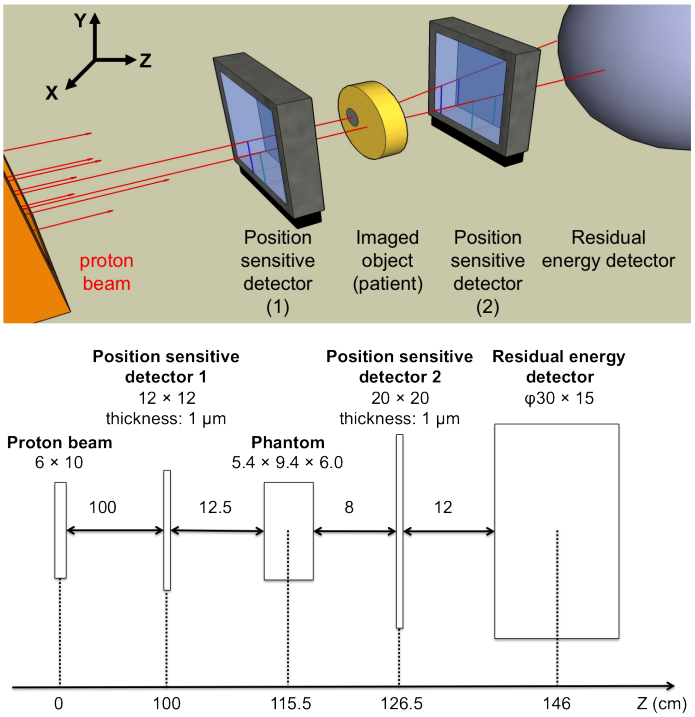

Figure 1. Top: proton radiography setup implemented in the Geant4 simulations including position sensitive and residual energy detectors. A few tracks of protons from the scattered beam are shown. Bottom: scheme of the proton radiography setup. All dimensions are in cm, unless specified otherwise.

individual proton were also increased to 12×12 cm^2 before and to 20×20 cm^2 after the phantom. The larger second position sensitive detector allowed measuring scattered protons with larger angles passing through the phantom materials with higher densities. The energy detector with a diameter of 30 cm and a thickness of 15 cm was filled with BaF_2 scintillator (crystal used in the proton radiography experiment) and it detected the residual energy of an individual proton.

2.2 Complex phantom

The phantom (made in-house), with dimensions $5.4 \times 9.4 \times 6.0$ cm^3 (x, y, z), consisted of polymethyl methacrylate (PMMA) and was filled with 6 inserts of different diameters and contents (figure 2(a)). The top insert (In6) was tilted, its top view can be seen in figure 2(b), while the other inserts were oriented parallel to the Z-axis, i.e. along the proton beam direction.

The phantom contains 11 different materials, including 6 tissue surrogates, such as: lung (Gammex 485), adipose (fat, Gammex 453), breast (Gammex 454), liver (Gammex 482), cortical bone (Gammex 450) and CT solid water (CTsw, Gammex 457) [10]. Three inserts (In2, In5, In6, figure 2(a)) in the phantom contain more than one type of material. Three metal implants of Al, Ti, and Cu are added to the insert filled with a cortical bone (In6) to mimic dental fillings (figure 2(b)). An air cavity (In2) and a lung tumor (PMMA in the lung tissue surrogate, In5) are also mimicked in the phantom. In this way, the geometry of the phantom is closer to a real patient geometry. Liver (In1) and breast (In3) are also included in the phantom, as these materials were not used in our previous studies. Densities of all phantom materials are presented in table 1.

2016 JINST 11 C12015

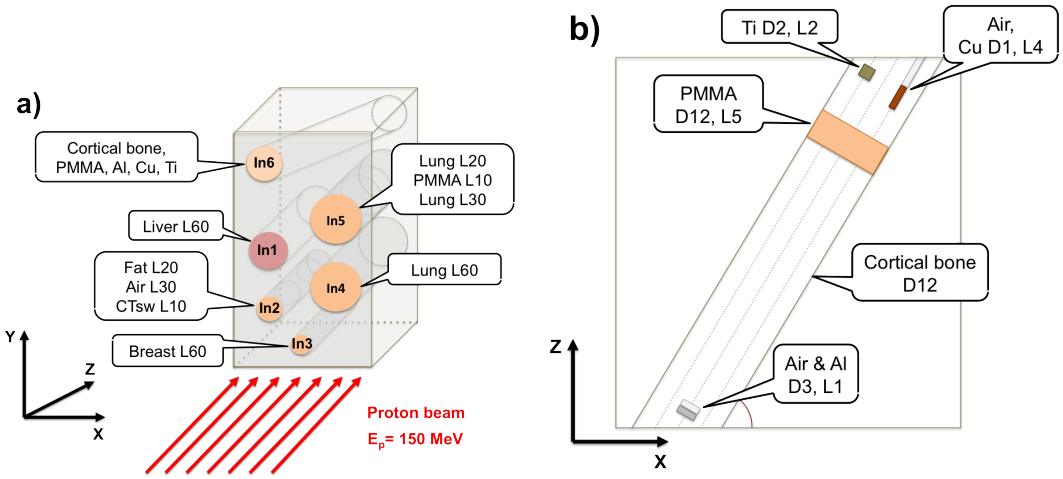

Figure 2. (a) The phantom used in the Geant4 simulations with 6 inserts of different sizes. Three inserts were filled with one tissue surrogate only: liver (In1), breast (In3), and lung (In4), with diameters of 15, 8 and 20 mm, respectively, and the thickness of 60 mm (L60). The other three inserts were filled with multiple materials: lung/PMMA/lung (In5), adipose/air/CTsw (In2), and cortical bone/PMMA/Al/Cu/Ti (In6) with diameters of 20, 10 and 12 mm, respectively, and various thicknesses with the total thickness for each insert of 60 mm. All dimensions are shown in mm. (b) Top view of a slice through the tilted insert (In6) with cortical bone, PMMA and metals.

Table 1. Physical densities of materials present in the phantom and implemented in the Geant4 simulations.

Phantom material	Physical density (g/cm^3)	Phantom material	Physical density (g/cm^3)
Lung*	0.428	Air	0.0012
Adipose (fat)*	0.946	PMMA	1.180
Brest*	0.981	Al	2.699
Liver*	1.095	Ti	4.510
CT solid water*	1.045	Cu	8.960
Cortical bone*	1.823	* Gammex (tissue-equivalent) materials [10]	

2.3 Physics list

In the simulations we used the Geant4.9.6p04 version with the standard electromagnetic physics, *G4EmStandardPhysics_option3()*. The default value of the *finalRange* parameter, which is included in the standard electromagnetic physics, describes the range for the final step and is used in the computation of the step limit by the ionization process. The *finalRange* parameter with a default value of 1 mm, is reduced for e^- and e^+ to 0.1 mm and for protons to 0.05 mm [11].

The model that is used in Geant4 for multiple scattering does not use the Molière formalism, but it is based on the more complete Lewis theory [12]. The scattering of a particle after a given step is simulated, and the path length correction and the lateral displacement are also computed. After each step, the angular and spatial distributions are determined. Any energy loss process in Geant4 must calculate the continuous and discrete energy loss in a material. Below a given energy threshold, which for secondary electrons varies between 55 keV and 250 keV in the materials used, the energy loss is continuous and above it the energy loss is simulated by the explicit production of secondary particles (gammas, e^- and e^+).

2016 JINST 11 C12015

2.4 Proton scattering angle

A proton passing through the phantom undergoes multiple Coulomb scattering (MCS) causing blurring of the radiography image. Similarly to our previous study [7], we calculated the scattering angle of a proton, ϕ, using momentum vectors before the phantom, $\vec{p}_0$ (p_{x0}, p_{y0}, p_{z0} obtained from Geant4 in the proton source) and after the phantom, $\vec{p}_3$ (p_{x3}, p_{y3}, p_{z3} obtained from Geant4 in the energy detector), as follows:

$$\phi(\text{rad}) = \cos^{-1} \frac{\vec{p}_0 \vec{p}_3}{|\vec{p}_0||\vec{p}_3|} \tag{2.1}$$

We applied various cuts on a proton scattering angle to minimize the blurring in the energy loss radiography image, discussed in the following section.

2.5 Energy radiographs and projections without and with cuts on proton scattering angle

The energy loss radiograph is created for protons that passed through all three detectors in the proton radiography system (figure 1). The energy loss of a proton, calculated for each of 10^6 generated protons, is the difference between the energy of an initial proton of E_p =150 MeV from the beam and the residual energy recorded in the energy detector after traversing the phantom, $\Delta E = E_{\text{beam}} - E_{\text{residual}}$. In the radiograph the average energy loss of protons $< \Delta E >$ is plotted versus the position. The obtained energy loss radiograph of the phantom, in which 99.98% of protons are considered, is shown in figure 3(a). The image is blurred due to MCS, but after selecting protons traveling along almost straight lines, for example, scattered no more than 5.2 mrad, all inserts with various materials in the phantom are clearly separated, as can be recognized in figure 3(b). A few white pixels are visible in the energy radiograph for scattered protons of up

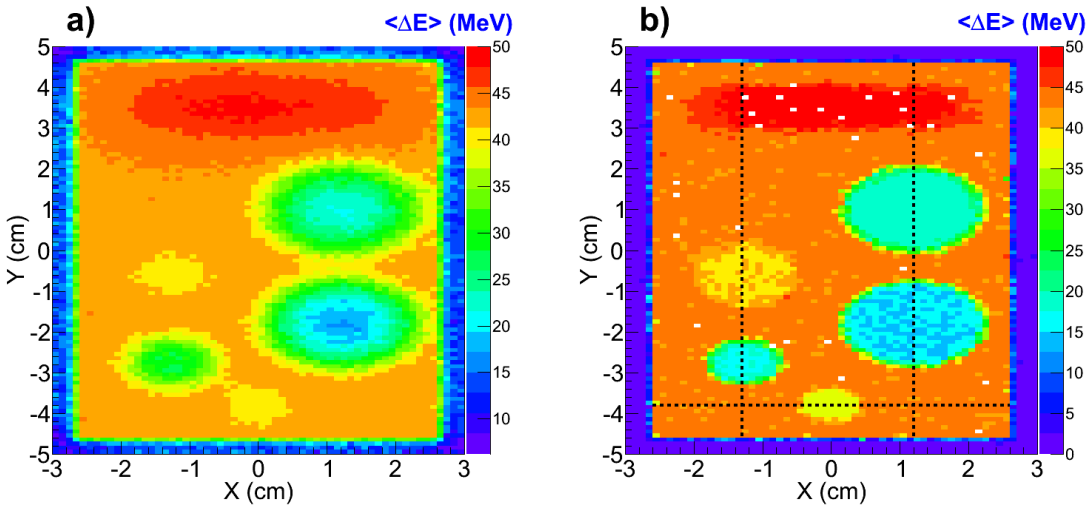

Figure 3. (a) The average energy loss radiograph using 99.98% of the generated 150 MeV protons that passed through all three detectors of the radiography system shown in figure 1. No cut on the proton scattering angle is applied. (b) The same energy loss radiograph as in figure 3(a) created for protons, which scattered only up to 5.2 mrad. Dashed lines mark bins of a size of 1 mm each at: $X = -1.3$ cm, $X = +1.2$ cm and $Y = -3.8$ cm, for which projections with various maximum proton scattering angles were made (shown in figure 4).

2016 JINST 11 C12015

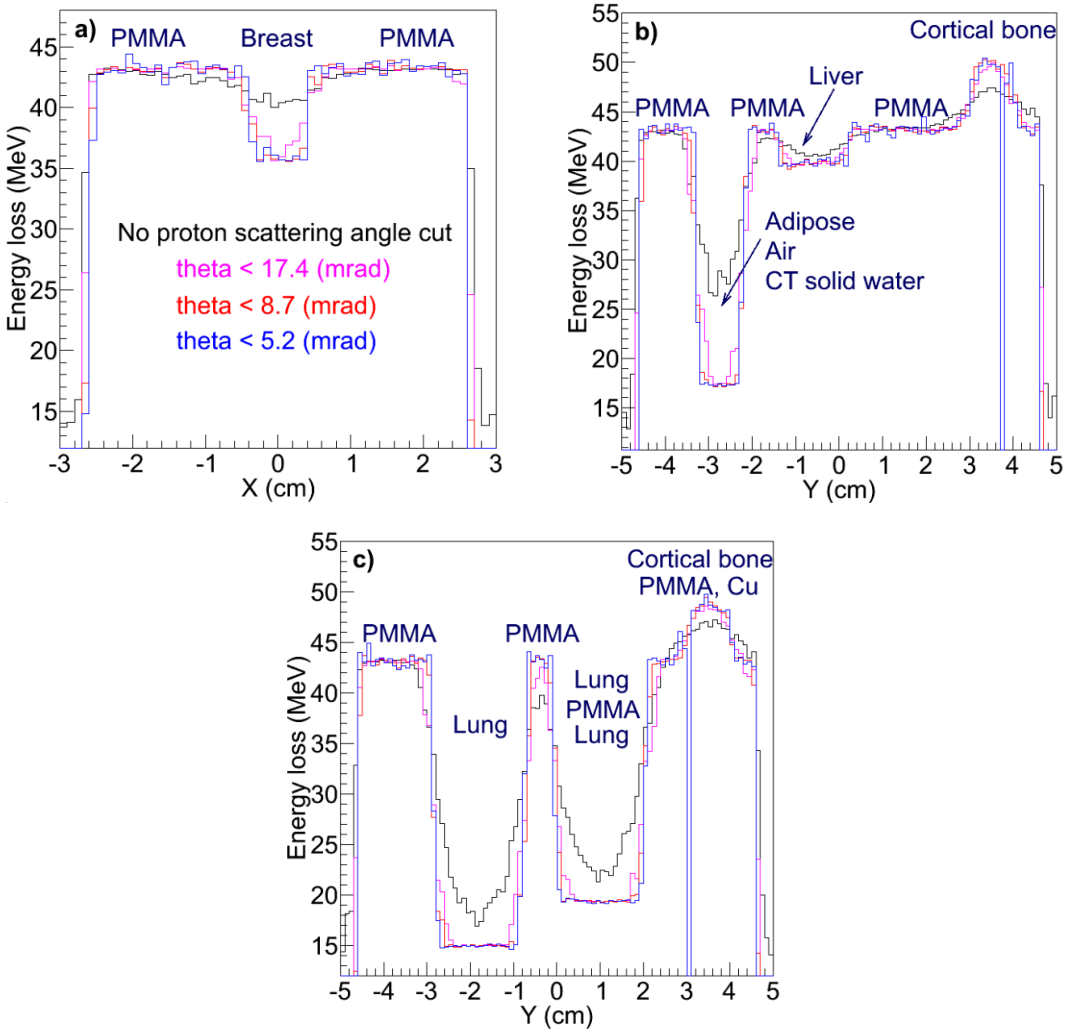

Figure 4. Projections through the phantom, as marked by dash lines in figure 3(b). Each projection is plotted for a bin size of 1 mm. The same colour for lines in all three plots 4(a), 4(b) and 4(c) represents the same cuts on maximum proton scattering angles, such as: all protons are considered, thus no cut on proton scattering angle is applied (black), protons with maximum scattering angles of up to 17.4 mrad (magenta), of up to 8.7 mrad (red) and of up to 5.2 mrad (blue) are considered.

to 5.2 mrad, which appeared due to a lack of statistics at this cut. The dashed lines in figure 3(b) at $X = -1.3$ cm, $X = +1.2$ cm and at $Y = -3.8$ cm represent examples of three bins, each of 1 mm size, for which projections at various maximum proton scattering angles were created, as demonstrated in figure 4. For the case with all protons considered to build the average energy loss radiograph, the image is blurred (figure 3(a)). The blur is also shown in the projections in figure 4 (black lines) as less sharp edges between various materials of the phantom. Sharper edges are observed for protons with scattering angles smaller than 8.7 mrad (red and blue lines in figure 4), thus for protons traveling almost along straight lines.

Applying cuts on proton scattering angle has an influence on the number of protons that are considered to build the average energy loss radiograph, as is presented in figure 5.

2016 JINST 11 C12015

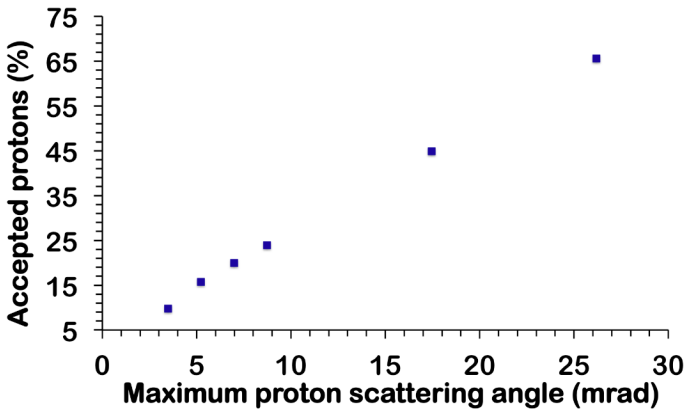

Figure 5. Accepted protons at various cuts on maximum proton scattering angle for a proton beam energy of $E_p = 150$ MeV.

Narrowing the selection of scattered protons (smaller maximum scattering angles of protons) decreases the number of protons considered in the image, as expected. Figure 5 shows that only 24% of protons have a scattering angle < 8.7 mrad. Thus, more than 70% of events are rejected. Nevertheless, in proton radiography imaging the energy of the proton beam is higher compared to the one used for proton radiotherapy treatment. At higher proton beam energies (of up to 250 MeV currently available for medical cyclotrons) protons scatter less, resulting in higher statistics at smaller scattering angles.

Even though it is evidently better to perform proton radiography at higher proton beam energies the first choice was made to perform the simulation at $E_p = 150$ MeV, because at this proton beam energy we have carried out the proton radiography experiment at the KVI-Center for Advanced Radiation Technology (KVI-CART) in Groningen. In this experiment the same phantom has been used (results from this experiment will be published elsewhere). The results presented in this paper for $E_p = 150$ MeV is not optimum, however, satisfactory.

3 Summary and future work

In this paper we present the analysis of the influence of proton scattering angles on the quality of proton energy loss radiography images for a larger and more complex phantom with 11 materials, including some tissue surrogates. To improve the image quality we select protons with small scattering angles. The results at proton beam energy of $E_p = 150$ MeV show that selecting protons that scattered up to 8.7 mrad give the sharpest edges in the energy loss radiograph, in which different materials can be recognized accurately, but at a cost of statistics. The number of events used to build the image was only 24%. The proton beam energy used in proton radiography imaging is, however, higher compared to the one used for proton treatment, thus the statistics will improve significantly for higher beam energies.

Our latest analysis additionally showed that calculating the scattering angle of protons using momentum vectors between position sensitive detectors before and after the phantom could improve the number of protons in the image by few %, and using the position of a proton instead of its momentum (as it is used in most of experiments), the statistics could be improved by a factor of 2.

2016 JINST 11 C12015

This analysis on using full information (including both momentum and position) of a proton is ongoing. Moreover, an alternative approach for using the proton scattering angle is being analysed, in which scattering angle distributions of protons in small voxels are analysed.

The next step is to use real patient data instead of a phantom in our Monte Carlo simulations, which in combination with X-ray CT will lead to more accurate relative stopping powers predictions.

Acknowledgments

We would like to thank the Center for Information Technology of the University of Groningen for their support and for providing access to the Peregrine high performance computing cluster, where the Monte Carlo simulations were performed. This work was partially supported by the Japan Society for Promotion of Science Core-to-Core Program (number 23003).

References

[1] T. Plautz et al., 200 *MeV proton radiography studies with a hand phantom using a prototype proton CT scanner*, *IEEE Trans. Med. Imag.* **33** (4) (2014) 875.

[2] V. Sipala et al., *A proton computed tomography system for medical applications*, 2013 *JINST* **8** C02021.

[3] H. Ryu et al., *Density and spatial resolutions of proton radiography using a range modulation technique*, *Phys. Med. Biol.* **53** (2008) 5461.

[4] U. Schneider and Eros Pedroni, *Multiple Coulomb scattering and spatial resolution in proton radiography*, *Med. Phys.* **21** (1994) 1657.

[5] G. Poludniowski, N.M. Allinson and P.M. Evans, *Proton radiography and tomography with application to proton therapy*, *Br. J. Radiol.* **88** (2015) 20150134, and references therein.

[6] A.K. Biegun et al., *Proton radiography with timepix based time projection chambers*, *IEEE Trans. Med. Imag.* **35** (2016) 1099.

[7] J. Takatsu et al., *Proton radiography to improve proton therapy treatment*, 2016 *JINST* **11** C01004.

[8] A.K. Biegun et al., *Proton radiography to improve proton radiotherapy: simulation study at different proton beam energies*, *Acta Phys. Pol.* **B 47** (2016) 329 [arXiv:1601.08074].

[9] GEANT4 collaboraiton, S. Agostinelli et al., *GEANT4 — A simulation toolkit*, *Nucl. Instr. Meth.* **A 506** (2003) 250.

[10] http://www.gammex.com/

[11] *Physics Lists EM constructors in Geant4 9.6 — Option 3*, http://geant4.web.cern.ch/geant4/collaboration/working_groups/electromagnetic/physlist9.6.shtml#opt3.

[12] *GEANT4 — Physics Reference Manual*, http://geant4.web.cern.ch/geant4/G4UsersDocuments/UsersGuides/PhysicsReferenceManual/html/.

2016 JINST 11 C12015